Neuroscience 594 (2026) 240–250

Contents lists available at ScienceDirect

Neuroscience

journal homepage: www.elsevier.com/locate/nsc

Efficiency and robustness in three cortical areas: frontal pole cortex, dorsolateral prefrontal cortex and orbitofrontal cortex

Davide Cipollini [a,1], Fabrizio Londei [b,c,1], Satoshi Tsujimoto [d], Francesco Ceccarelli [b,e,*], Aldo Genovesio [b,e,f,*]

[a] Advanced Materials Metrology and Life Sciences Division, INRiM (Istituto Nazionale di Ricerca Metrologica), 10135 Torino, Italy
[b] Department of Physiology and Pharmacology, Sapienza University of Rome, Piazzale Aldo Moro 5, 00185 Rome, Italy
[c] Behavioral Neuroscience PhD Program, Sapienza University, Rome, Italy
[d] SixthFactor Pte. Ltd, Singapore
[e] Institute of Biochemistry and Cell Biology (IBBC), National Research Council of Italy (CNR), Via Ramarini 32, 00015 Monterotondo Scalo, Roma, Italy
[f] Department of Pharmaceutical Sciences, University of Eastern Piedmont Amadeo Avogadro, Novara, Italy

ARTICLE INFO

Keywords:
Efficiency
Robustness
Evolution
Frontal pole cortex
Dorsolateral prefrontal cortex
Orbitofrontal cortex

ABSTRACT

The prefrontal cortex in primates has a diverse evolutionary history, characterized by distinct phases of development. Granular regions of the orbital prefrontal cortex (PFo) emerged early in primate evolution, while other granular areas, such as the dorsolateral (PFdl) and polar (PFp) regions, evolved later during anthropoid development. This study explored the functional differences among PFp, PFdl, and PFo in macaque monkeys, focusing on their coding mechanisms, specifically regarding robustness and efficiency. Efficiency was estimated using the 'contrast entropy', defined as the entropy of the neuronal spiking activity normalized by the expected theoretical maximum, whereas robustness was estimated as the synchrony of activity between neurons within the same area. Our investigation revealed that PFp and PFdl show superior information capacity, reflecting efficient coding compared to PFo. Conversely, PFo exhibited higher robustness, suggesting a trade-off relationship between efficiency and robustness consistent with distinct evolutionary stages. The newly incorporated granular prefrontal cortex regions, namely PFp and PFdl, appear to employ a more highly efficient neural code at the expense of reliability, as evidenced by lower robustness.

Introduction

The prefrontal (PF) cortex exhibits evolutionary dynamism and diversity, with new areas and connectivity systems developing in phases. One such phase occurred in early mammals, giving rise to the agranular regions of the PF cortex, which are shared among virtually all mammals (Preuss, 2001; Wise, 2008; Preuss and Wise, 2022). In contrast, the granular PF cortex evolved in later stages, particularly during primate evolution (Preuss, 2007). Specifically, the granular components of the orbital PF cortex (PFo) and the caudal PF cortex (Brodmann area 8), including the frontal eye field (FEF), emerged in early primates (i.e., strepsirrhines), followed by a later phase of granular PF expansion during anthropoid evolution (Preuss and Goldman-Rakic, 1991; Wong and Kaas, 2010). Notably, this later phase introduced areas primarily anterior to the FEF, such as the dorsolateral PF cortex (PFdl) and the polar PF cortex (PFp), among others (Passingham and Wise, 2012; Preuss and Wise, 2022). In line with these primate evolution processes, the new addition of these granular PF areas conferred adaptive advantages in dynamic and complex environments by enabling flexible cognitive and behavioral control and facilitating rapid learning based on single experiences (Miller and Cohen, 2001; Mansouri et al., 2017), while the granular PFo appears more involved in value- and object-based action selection (Wallis, 2007; Rudebeck and Izquierdo, 2022). Furthermore, and perhaps relatedly, these newly added granular PF areas, particularly the PFdl, have been implicated in various psychiatric disorders, in particular schizophrenia (Selemon and Zecevic, 2015; Smucny et al., 2022). It is therefore important to understand what evolutionary changes, if any, accompanied the addition of new prefrontal areas in primate evolution.

While previous investigations of evolutionary differences have

* Corresponding authors.
E-mail addresses: francesco.ceccarelli@uniroma1.it (F. Ceccarelli), aldo.genovesio@uniupo.it (A. Genovesio).
[1] These authors contributed equally to this work.

https://doi.org/10.1016/j.neuroscience.2025.12.047
Received 5 June 2025; Accepted 16 December 2025
Available online 17 December 2025

mostly focused on the neuroanatomical differences, Pryluk et al. (2019) recently introduced basic features of the neural code, specifically efficiency and robustness, as measures for exploring evolutionarily driven differences across brain regions and species. In this context, efficiency is a measure of the information capacity in a channel (i.e., a neuron), while the synchrony between neurons estimates robustness within the same cortical area. Both measures are assumed to result from adaptive pressure but in somewhat opposite ways. Specifically, robustness supports the speed and vigor of responses, which are necessary for reliable execution of basic survival responses, while efficiency allows better exploitation of information capacity and the complex use of neural vocabulary, which are advantageous for flexible adaptation and learning in new environments. Consistent with this assumption, a 'tradeoff' between efficiency and robustness was found across species and brain structures, suggesting a shift from robustness towards efficiency parallel to evolutionary processes (Pryluk et al., 2019).

The present study aims to investigate these basic neural coding mechanisms across three granular PF areas that have evolved at different phases, specifically contrasting PFp and PFdl with PFo. In a series of previous studies, we have both investigated each PF area individually and also compared various aspects of neural activities across these PF areas, including task-related firing activities (Tsujimoto et al., 2010, 2012; Marcos et al., 2019; Ferrucci et al., 2022a; Ceccarelli et al., 2023), trial-to-trial variability (Tsujimoto and Genovesio, 2017), and temporal receptive fields of the neurons (Fascianelli et al., 2019). Among the neurons recorded and analyzed in these studies, here we calculate the efficiency by the entropy rates normalized to the theoretical limit (Shannon, 1997) of the channel under inquiry, so that the information capacity of neurons can be quantified across different areas (Pryluk et al., 2019). In addition, to estimate the robustness of the neural code, we computed the Pearson correlation of the discretized spiking activity of simultaneously recorded neurons belonging to the same area, as well as the synchronous time lag. We report that PFp and PFdl showed superior efficiency in neural coding compared to PFo, while PFo exhibited higher robustness, suggesting a trade-off relationship between efficiency and robustness consistent with distinct evolutionary stages.

Methods

Subjects

Two adult male rhesus monkeys (Macaca mulatta), weighing 10–11 kg, were trained to perform the tasks before the recordings. During the task, each monkey was seated in a primate chair with their head stabilized and facing a video monitor positioned 32 cm away. An infrared oculometer (Arrington Research, Inc., Scottsdale, AZ) was used to track their eye position. All experimental procedures were in agreement with the Guide for the Care and Use of Laboratory Animals and were approved by the National Institute of Mental Health Animal Care and Use Committee.

Data collection

After the tasks training was completed, a craniotomy was performed to expose the dura mater of the left hemisphere above the PFp and to implant a custom-made recording chamber (10.65 mm inner diameter) designed to fit the entry hole to the recording site. Surgical techniques and a detailed description of the PFp chamber were reported previously (Mitz et al., 2009). Following data collection with PFp, MRI was employed to determine the angle and position for implanting an additional chamber (18 mm inner diameter) in a more caudal location within the same hemisphere, which could simultaneously have access to PFo and PFdl. In this case, usually half of the 16 electrodes employed were positioned in PFdl, and the remaining advanced deeper to reach PFo (Tsujimoto et al., 2011). Standard histological analysis and structural MRI were used to reconstruct the recording sites in the three areas of interest. Near the end of the recordings, electrolytic lesions (20 A for 20 s, anodal current) were applied at designated locations and at two depths in the caudal chamber. At 10 days after this procedure, under induced deep anesthesia, the animals were perfused with 10 % (v/v) formol saline to the heart. During perfusion, a pin was inserted centrally into both recording chambers. Pins and electrolytic lesions were then taken as references in the Nissl-stained sections to reconstruct the recording sites. Recording sites in PFdl were located in both animals at the level of the dorsal bank of the principal sulcus, with further sites at the level of the ventral bank collected only in one animal (Tsujimoto et al., 2009; Fascianelli et al., 2024). The sites in PFp involved the dorsomedial part of Brodmann area 10 (Walker, 1940). In both monkeys, the sites were confined to a limited area (5 mm), with a higher site density bias in the caudomedial and rostrolateral region in the two monkeys, respectively (Tsujimoto et al., 2010). In PFo, recording sites were partially dissimilar between monkeys: more lateral and rostral sites in monkey 1 originated from the ventral portions of areas 12 and 11, whereas in monkey 2 sites were mainly from area 13. Cytoarchitectonic analyses confirmed that the PFo sites originated from the granular (i.e., homotypical) prefrontal cortex (Tsujimoto et al., 2009). Previous studies have illustrated the recording sites for PFdl (Tsujimoto et al., 2011; Fascianelli et al., 2024), PFp (Tsujimoto et al., 2010), and PFo (Tsujimoto et al., 2009). Simultaneous recording of single-cell activity was performed using up to 16 platinum-iridium electrodes (0.5–1.5 MΩ at 1 kHz; Thomas Recording, Giessen, Germany). The electrodes were inserted individually using a multielectrode drive (Thomas Recording), providing independent control over their positions. The horizontal spacing between the 16 electrodes could range from 305 μm to approximately 2 mm depending on the electrode spacing within the microdrive system. However, a further increase in the distance between the electrodes might result from the advancement of the electrodes at different depths.

The signals from each electrode were recorded using a Multichannel Acquisition Processor (Plexon, Dallas, TX). Single-cell potentials were initially isolated online and further sorted offline using a cluster cutting technique (Off Line Sorter, Plexon). The sorting process involved multiple criteria, including principal component analysis (PCA), minimal interspike intervals, and thorough visual inspection of the complete waveforms for each cell.

Behavioral task

The dataset employed in this study included daily recordings of three behavioral tasks, sequentially performed under a block design, with about 60–100 trials per task. Recordings usually began with the visually cued strategy task, followed by the fluid-reward cued strategy task, and then ended with the delayed-response task, as previously described in Tsujimoto et al. (Tsujimoto et al., 2010, 2011, 2012). Each trial began with a 1-second inter-trial interval, followed by the presentation of a fixation point (a 0.6° filled white circle) at the center of the video screen, together with two potential saccade targets (2.0° unfilled white squares) located 11.6° to the left and right of the fixation point.

The monkeys were required to attain and maintain fixation on the central point for 1.5 s to initiate a trial. Subsequently, the initial fixation period was followed by a cue period of 0.5 s. The nature of the cue varied depending on the task (Fig. 1B) and could either be a visual cue or a fluid-reward cue. In the visually cued strategy task, the cue appeared as a square (2.0° × 2.0°) or a rectangle (1.0° × 4.9°) at the fixation point (Fig. 1B). In each trial a cue was randomly selected from a set of four possibilities: a vertical rectangle (light gray), a horizontally oriented rectangle with the same dimensions and brightness, a yellow square, or a purple square, all of the same size (Fig. 1B).

In the fluid-reward cued strategy task, instead of a visual stimulus, a cue was delivered at the beginning of the cue period (Fig. 1B) as either a single drop of fluid (0.2 ml) or two half-drops of fluid (0.1 ml each), the "stay cues," which included the yellow square, the vertical rectangle,

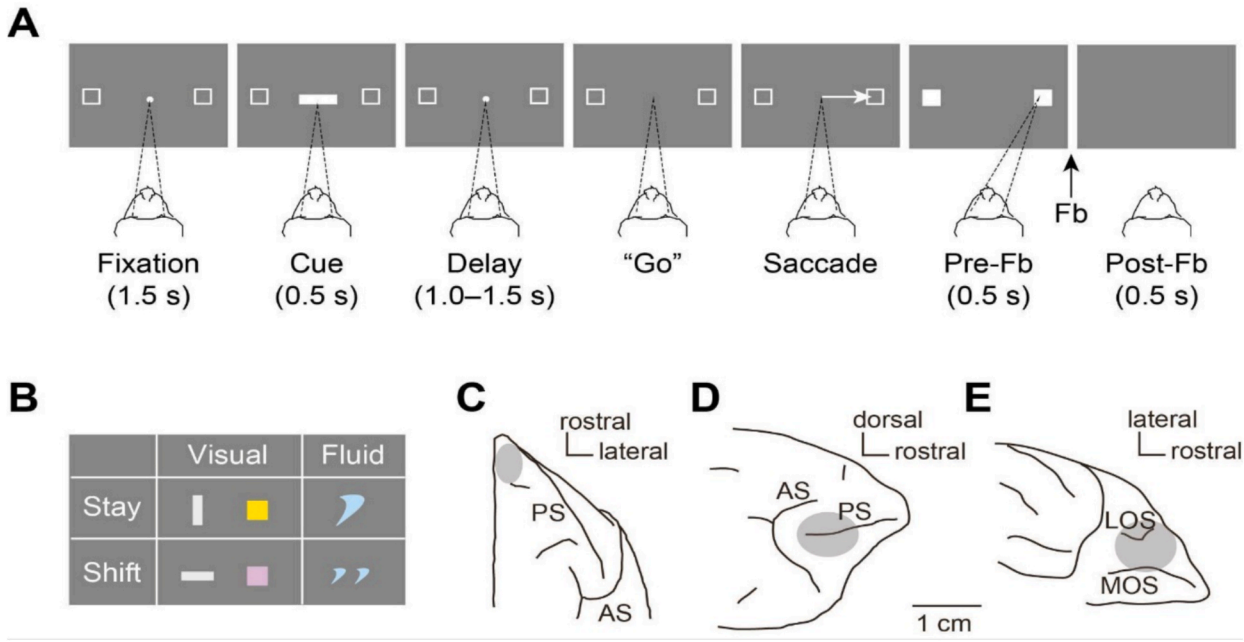

Fig. 1. Cued strategy task, cue types, and recording sites. (A) Sequence of task events. The dark gray rectangles are the video screen as viewed by the monkey. The dashed lines indicate the monkey's gaze. (B) Visual and fluid strategy cues presented to the monkey. Each different color, shape, and number of drops of fluid instructed the strategy to be applied. (C), (D), (E), Recording area for PFp (C), PFdl (D), and PFo (E). Fb, Feedback; LOS, lateral orbital sulcus; MOS, medial orbital sulcus; AS, arcuate sulcus; PS, principal sulcus. Figure adapted from Fascianelli et al. (2019).

and one drop of fluid, instructed the monkeys to adopt a "stay" strategy, selecting the same response as on the previous trial. The "shift cues", consisting of the horizontal rectangle, purple square, and two half-drops of fluid, instructed the monkeys to adopt a "shift" strategy, requiring them to switch from their previous response. We also used a third task, the delayed-response task (not shown) in which a 0.6° filled white circle was presented inside either the left or right target square. This visuo-spatial cue indicated the correct target. The right and left trials were intermixed pseudorandomly with equal probability. Throughout the tasks, the monkeys were required to maintain fixation on the central spot for the entire cue period, as well as during a subsequent delay period (where the cue was turned off) of either 1.0, 1.25, or 1.5 s, which was selected pseudorandomly. The fixation spot and the two potential saccade targets remained visible on the screen throughout the delay period. The go signal to initiate a saccadic eye movement towards one of the targets was represented by the disappearance of the fixation spot. Once the monkey's saccade fell within a window of $\pm$ 3.75° centered on either target, both targets turned solid white, both in correct and error trials. The monkey had to maintain fixation on the target for 0.5 s. Once target fixation exceeded 0.5 s, a single drop of fluid (0.2 ml) was delivered as reward feedback for correct responses. In case of errors, the presentation of red squares over both targets provided negative feedback. After errors, the cue from the previous trial was repeated on a correction trial, which continued until the monkey responded correctly and obtained a reward in the correction trials. The three tasks were presented in separate blocks of trials. We recorded some variations of the three tasks in a limited number of sessions, characterized by a longer duration of the following epochs: Pre-Fb (1 sec), Post-Fb (1 sec), and inter-trial interval (1.5 sec). Finally, in some sessions of the fluid-reward cued task, the reward feedback, similar to the cues used for that task, was either a single drop of fluid (0.2 ml) or two half-drops (0.1 ml each), selected pseudorandomly.

Dataset

From the original dataset described in Tsujimoto et al. (2010, 2011, 2012), we selected 522 single neurons and 192 pairs of simultaneously recorded neurons for each of the recorded areas in order to match the number of neurons and pairs of neurons in the three regions and reduce the differences in firing rates. Specifically, we selected only neurons and pairs of neurons with similar firing rates, which means with a difference in firing rates less than a threshold set at 0.1 Hz (see *Selection of neurons and pairs with similar firing rate* for a detailed description of the selection criteria). The neurons included in the populations selected for each area were recorded in at least one of the three tasks recorded daily, with the great majority, 77.6 %, recorded only in one task, 20.3 % in two tasks, and 2.1 % in all three tasks. Neurons recorded in multiple tasks were considered independently and taken more than once in the selected population. PFo neurons were organized in 229 sessions, PFdl neurons in 215 sessions, and PFp neurons in 259 sessions. All the regions have a median of 2 neurons per session, spanning between a minimum of 1 neuron to a maximum of 7 neurons recorded simultaneously in a single session. For the following analyses that considered single-cell activity, we used the entire recording in which the cell was recorded. For analyses on cell pairs, we used the portion of the recording in which both cells were recorded simultaneously.

Neural code robustness and efficiency

In order to quantify the robustness of the neural code, two metrics were used. The first metric employed is the Pearson correlation coefficient of the discretized spiking activity of neurons simultaneously recorded and belonging to the same area. The second metric is the synchronous time lag calculated by cross-correlation between spike trains of neuron pairs, as in Pryluk et al. (2019). Specifically, spike trains were initially binned by using word lists consisting of the possible combinations of letters W and $\Delta\tau$, where each word spanned $T = W\Delta\tau$. In this context, $\Delta\tau$ dictated the bin size and W the temporal extension of the spike train segmentation. Then, the optimal lag was calculated over the flattened sequences as the peak location of the cross-correlation between the two spike trains, limiting the possible shift of the two neurons to the range of W. Consequently, the synchronous time lag is

equivalent to that optimal lag multiplied by the bin size $\Delta\tau$, and is upper bounded by the maximum length of a word. In order to quantify the efficiency, we use the contrast entropy (Pryluk et al., 2019), designed to estimate the information capacity of neurons based on the entropic expressivity of the neural code, considering the natural constraint of each neuron's firing rate capacity. For the sake of completeness, we dedicate the next Section to the contrast entropy, providing the necessary background for this work.

Contrast entropy

The entropy rate of a spike train, as described by Borst & Theunissen (1999), provides an indicator of a neuron's ability to transmit information. This rate increases as the firing rate goes up, and the firing rate sets an upper limit on the entropy rate (Pryluk et al., 2019). However, it is important to note that the firing rate alone does not completely characterize the entropy, as the timing of each spike plays a crucial role in determining the actual entropy of a spike train and the information capacity of the channel that generated the signal (Rieke et al., 1999). As discussed by Pryluk et al. (2019), to uncover differences in the neural code of distinct areas, it is crucial to normalize the channel's capacity for transmitting information relative to the firing rate, which is constrained by both local and global factors. In other words, we need an information capacity metric that is possibly orthogonal to the firing rate. This allows us to compare different areas with different firing rates and assess how much neurons make the most out of their information transmission capabilities. To this purpose, Pryluk et al. (2019) developed a novel information theoretical tool named *contrast entropy*, (*CE*), which is the ratio between the entropy, *Ent*, computed over the neuron spike train and the theoretical maximal entropy, $Ent_{\max}$, of an analytic neuron with the same firing rate:

$$CE = \frac{Ent}{Ent_{max}} \tag{1}$$

where *CE* is bounded between 0 and 1 by definition. To compute the entropy, the spike train of the neuron is discretized into bins of temporal length $\Delta\tau$, each bin is a binary letter (Strong et al., 1998; Rieke et al., 1999). Each letter takes either the value 1, if at least one spike occurred in the time bin of $\Delta\tau$, or 0, if no spike occurred. A word is defined by a number W of letters. A word has temporal length $T = W\Delta\tau$. The probability, p_i, of occurrences of the i^{th} word is defined as its number of occurrences normalized by the total number of words occurring. Thus, the entropy rate equals to:

$$Ent = -\frac{\sum_i p_i \log_2 p_i}{T} \tag{2}$$

The maximum entropy that can be obtained from a spike train with the same firing rate is defined as the one entropy we would obtain when each spike occurs as an identically distributed independent event with probability $p_S = \bar{r}\Delta\tau$:

$$Ent_{max} = -\frac{\sum_{i=0}^{W} C_i^W p_S^i (1-p_S)^{W-i} \log_2\left(p_S^i (1-p_S)^{W-i}\right)}{T} \tag{3}$$

where $\bar{r}$ is the mean firing rate and $C_i^W = W!\,/\,(W-i)!\,i!$ is the number of possible words of W-letters with i-number of letters equal to 1. As information theoretical measures are prone to upward bias due to limited data sampling (Treves and Panzeri, 1995), we used the approach from Strong et al. (1998) to correct it. Note that the analytic entropy of Equation (3) is not affected by the sampling bias. Thus, the upward bias affects the contrast entropy *CE* solely via the naive entropy.

The correction method from Strong et al. (1998) relies on the estimation of the entropy at infinite-word length. The method proceeds as follows:

1. For each neuron, we compute the naive entropy rate, *Ent*, for a fixed value of $\Delta\tau$ (the letter time length) and for multiple values of W (the number of letters in a word). For the single neuron, we use $W = 4,6,8,16$. Note that in Sections 2.5.2 and 3.2.2, for the analyses of neuron pairs, we will use $W = 2,4,6,8$, for computational reasons.
2. The computed entropy is plotted as a function of the inverse word length, $1/T = 1/(W\Delta\tau)$.
3. The y-intercept obtained through linear regression defines the neuron's entropy estimated at infinite word length, for fixed $\Delta\tau$. We then average across all neurons, and the resulting value is plotted as a function of $\Delta\tau$ (see Fig. 2A).

In all parts of this work, the contrast entropy values presented are calculated using the entropy rate at infinite word length, instead of the naive entropy *Ent*, in the numerator of Equation (1).

Entropy for pairs of neurons

To confirm that the properties of the neural code are not exclusive to individual neurons within the examined PF areas but are also attributes of the prefrontal area's network, we estimate the contrast entropy for pairs of neurons that were simultaneously recorded and belong to the same PF area. We used the two metrics introduced by Pryluk et al. (2019). The *pairs contrast entropy* is computed by discretizing the spike train of the two neurons belonging to one pair, see Section 2.6, and then creating a joint word of $2W$ number of letters. The probability of a word with i-spikes and j-spikes from the first neuron and the second neuron respectively is:

$$P_{pair}(i,j) = p_{S_1}^i \left(1-p_{S_1}\right)^{W-i} p_{S_2}^j \left(1-p_{S_2}\right)^{W-j} \tag{4}$$

The maximum analytic entropy expressed by the pair is:

$$Ent_{max.pair} = -\sum_i \sum_j C_i^W C_j^W P_{pair}(i,j) \log_2 P_{pair}(i,j) \tag{5}$$

The naive contrast entropy is then defined as:

$$CE_{pairs} = \frac{Ent_{pairs}}{Ent_{max.pairs}} \tag{6}$$

where Ent_{pairs} is the pair (naive) entropy of words' distribution after combining the i^{th} word with the j^{th} word of the first and the second neuron, respectively. It follows $Ent_{pairs} \in [0,1]$.

For every neuron, we also estimate the *combined contrast entropy*, that is the sum of the contrast entropy in Equation (1) computed for both neurons in the pairs:

$$CE_{\text{comb}} = CE_1 + CE_2 \tag{7}$$

As for the single-neuron case, in the contrast entropy of Equation (6) and (7), the naive entropy is replaced with the estimated entropy at infinite word length from Strong et al. (1998). The method is analogous to the one described at the end of Section 2.5.1, with the only difference that, rather than using the entropy for the single neuron, we use the entropy for each pair of neurons. Note that once the method of Strong et al. (1998) is applied, the infinite-word-length entropy is a function of the letter time length $\Delta\tau$ only (see Fig. 5A).

Selection of neurons and pairs with similar firing rate

To reduce differences in firing rates and obtain populations of neurons and pairs of equal size, we developed a subsampling technique similar to that described by Pryluk et al. (2019). Nevertheless, our technique is designed to be applied to three distinct regions, rather than a couple of regions. As outlined in the aforementioned study, we initially identified the cortical regions with the lowest number of neurons. Then, for each neuron recorded in this area, we paired it with all neurons in one of the other two groups that had a firing rate distance less than the

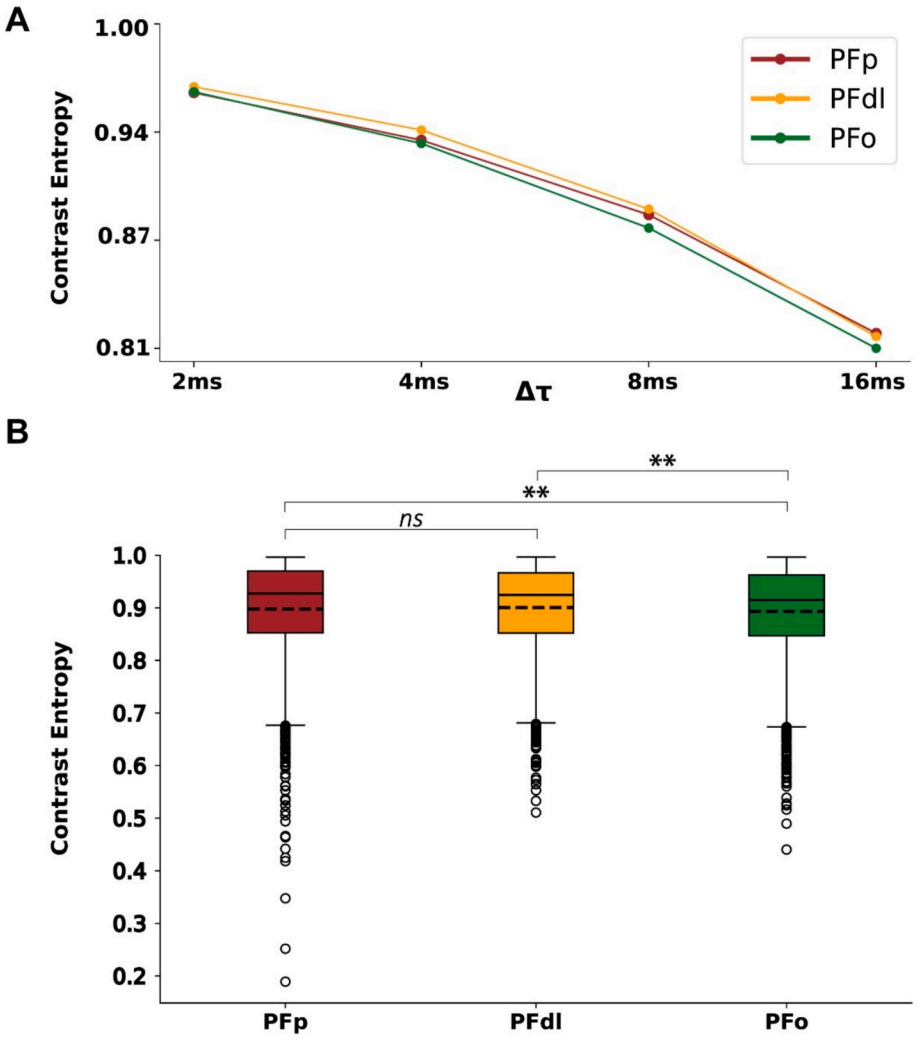

Fig. 2. Single neuron average contrast entropy for each PF area. (A) Contrast entropy estimated at infinite word length (Strong et al., 1998) is plotted as a function of letter time-bin $\Delta\tau$ for each cortical region (legend). Higher contrast entropy (higher efficiency) is measured for PFp and PFdl when compared to PFo. (B) The distribution of measured contrast entropy is shown for each area after aggregating measurements for all values of $\Delta\tau$. The dashed and continuous black lines indicate the distributions' mean and median, respectively. The box depicts points included between the first quartile (Q1) and the third quartile (Q3). Whiskers are drawn from the box to the farthest data point lying within the 1.5x the inter quartile range (IQR). Data points outside of the whiskers are plotted as outliers. The Mann–Whitney *U* test between couples of distributions is shown on top. Significant differences are observed in PFo in comparison with both PFdl and PFp. We use W = 4, 6, 8, 16 to estimate the infinite word length contrast entropy. * $p < 0.05$; ** $p < 0.01$; *** $p < 0.001$; ns non-significant.

threshold set to 0.1 Hz, following the approach in Pryluk et al. (2019). Note that this firing rate was calculated on the entire recording. At this point, for each couple identified in the previous step, we have identified all neurons in the remaining group whose firing rate distance was below the threshold with respect to both the neurons in the couple, consisting of one neuron from the first group and one from the second. This operation was performed for both groups with higher cardinality. In this way, we created triplets of neurons with the following properties:

1. each neuron belongs to a different PF area;
2. two by two, the neurons have a difference in the average firing rate less than the chosen threshold.

Next, we associated each triplet with the maximum distance in firing rate between two of its three component neurons, a distance that by construction is surely less than the chosen threshold and sorted the triplets according to this value. We then selected the triplet with the smallest maximum distance, removed its three component neurons from the dataset, and repeated the procedure again from the beginning on the updated dataset. This procedure was repeated until all neurons in the smallest group were removed or it was impossible, with the remaining neurons, to construct other triplets with the properties described above. Through this subsampling procedure, we selected 522 triplets of neurons with similar firing rate and thus three groups of 522 neurons, one for the PFo, one for the PFdl, and one for the PFp. Besides selecting only neurons whose maximum distance in the firing rate was less than 0.1 Hz, this procedure ensures that exactly the same number of neurons are selected for each cortical area.

Regarding the selection of pairs of neurons, we operated equivalently but with the inevitable adjustments to handle two neurons each time. Therefore, we first sorted the two neurons in each pair according to firing rate, thus identifying the one with the lower and the higher firing rates. Then, instead of selecting all neurons at a distance less than 0.1 Hz, we selected all pairs of neurons such that:

1. Two by two, the neurons with lower firing rate had a difference of less than 0.1 Hz;

2. Two by two, the neurons with higher firing rate had a difference of less than 0.1 Hz;
3. The sum of these differences in the firing rate was less than 0.1 Hz.

Note that at the end of our selection process, we obtain distributions of couples of equal size.

Results

To compare the efficiency and robustness of the three different prefrontal areas and maximize the size of the dataset used in all the analyses performed, we used all the data available from all three tasks as described in Methods. At the same time, since variations in firing rates can impact correlation-related analyses and entropy calculations (Cohen and Kohn, 2011), we implemented a subsampling technique to reduce differences in firing rates of individual neurons and pairs of neurons used in our analysis. Moreover, this way, we equalized the number of neurons across the three brain-specific areas. At the end of the subsampling procedure, we selected 522 neurons and 192 pairs of simultaneously recorded neurons for each of the brain areas considered.

Single neuron

Fig. 2A shows the neural code efficiency of the three PF areas, indexed by the contrast entropy estimated for infinite word length. Overall, high efficiency ($CE > 0.8$ even at the letter time-bin of 16 ms) was observed for all three PF areas examined. Across letter time bins ($\Delta\tau$), contrast entropy decreased with coarser discretization of the spike trains, i.e., for larger $\Delta\tau$. This occurs because coarser discretization reduces the temporal resolution of the spike patterns. Consequently, temporal correlations between adjacent words increase, and the overall entropy decreases (Treves and Panzeri, 1995).

To quantitatively assess the regional differences in neural code efficiency, the box plots in Fig. 2B show the distributions of single-neuron contrast entropy measured for each individual PF area. The significance of the differences was assessed using the Mann–Whitney *U* test. We found that PFo was the area with the lowest efficiency when compared to PFdl ($p = 0.0082$, U = 2282847) and PFp ($p = 0.0017$, U = 2302262), which together constituted the prefrontal areas with the highest efficiency and did not differ significantly from each other ($p = 0.5516$, U = 2203068).

Neuron pairs

To extend our findings beyond the single neuron case, we investigated the efficiency as a property of the network. We measured the efficiency and robustness between pairs of neurons belonging to the same prefrontal area. To compare the three PF areas, we selected distributions of neurons with similar firing rate in order to further mitigate the effect of the firing rate in our analysis, following the methodology proposed in Pryluk et al. (2019) (see Methods). Fig. 3 shows the density function of simultaneous-recording time intervals per pair. Using these pairs, we examine robustness and efficiency below.

Robustness in pairs of neurons

Fig. 4 illustrates the estimated robustness of the three PF areas, indexed by the Pearson correlation and the synchrony time lag between neuron pairs.

The cumulative density function (CDF) of the Pearson correlation in Fig. 4A shows a more reliable population response and higher robustness for the PFo (green) when compared to the PFp (red) and the PFdl (yellow). The difference between PFo and the other two regions was statistically significant (Mann-Whitney *U* test; PFp vs PFo: $p = 5.5\text{x}10^{-4}$, U = 4472650; PFdl vs PFo: $p = 0.0154$, U = 4550252; Fig. 4C), while no statistically significant difference was observed between the PFp and the PFdl ($p = 0.2946$, U = 4639658).

The CDF of synchrony time lag in Fig. 4B shows a faster saturation for the PFo when compared to the PFp and PFdl. As shown in Fig. 4D, synchrony in the activity of the neuron population may be interpreted in terms of better downstream summation and faster as well as more reliable responses for the PFo area (Mann-Whitney *U* test; PFp vs PFo: $p = 0.0017$, U = 4929323; PFdl vs PFo: $p = 0.2328$, U = 4801035; PFp vs PFdl: $p = 0.0761$, U = 4835004).

Efficiency in pairs of neurons

As for the single neuron analysis described above, we estimated the contrast entropy at infinite word length for neuron pairs following the method proposed by Strong et al. (1998) and described in Methods. The contrast entropy at infinite word length is obtained using the dependence of *Ent* and Ent_{pair} from *W* to provide an estimate that depends only on the time-bin of the letter $\Delta\tau$ (see Fig. 5A). We measured the pair-contrast entropy, which revealed a consistent trend of higher efficiency for PFp and PFdl compared to PFo across the explored range of $\Delta\tau$ (Fig. 5A). Statistical testing confirmed this trend (Fig. 5B), with PFo demonstrating significantly different distribution of pair *CE* than those of PFdl ($p = 0.0024$, U = 321259) and PFp ($p = 0.0014$, U = 322636), and no significant difference between the latter two ($p = 0.7813$, U = 297325). The pair-contrast entropy was consistent with the single

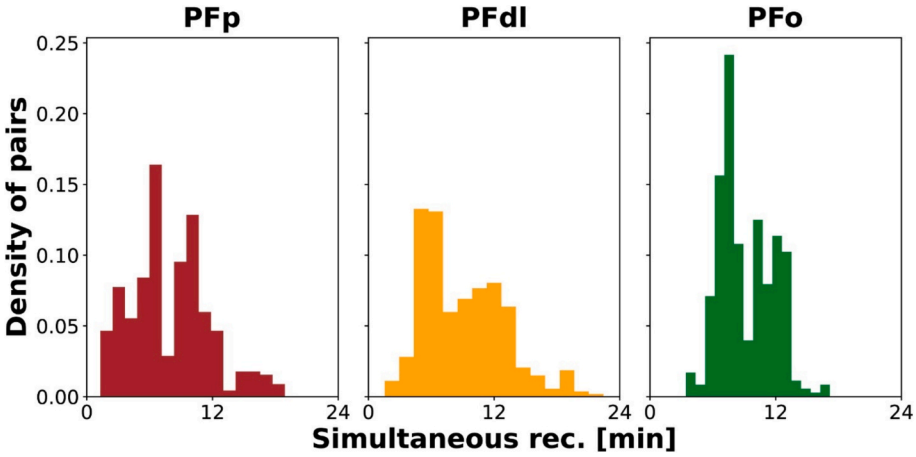

Fig. 3. Density function of simultaneous recording per neuron-pair resulted from the subsampling method described in Section 2.6. Our subsampling method ensures that an equal number of pairs (192) is chosen for each PF region. The 24-minute window has solely visualization purposes. It corresponds to the rounded-up maximum duration of simultaneous recordings observed between any two neurons (specifically, in pairs of neurons within PFdl).

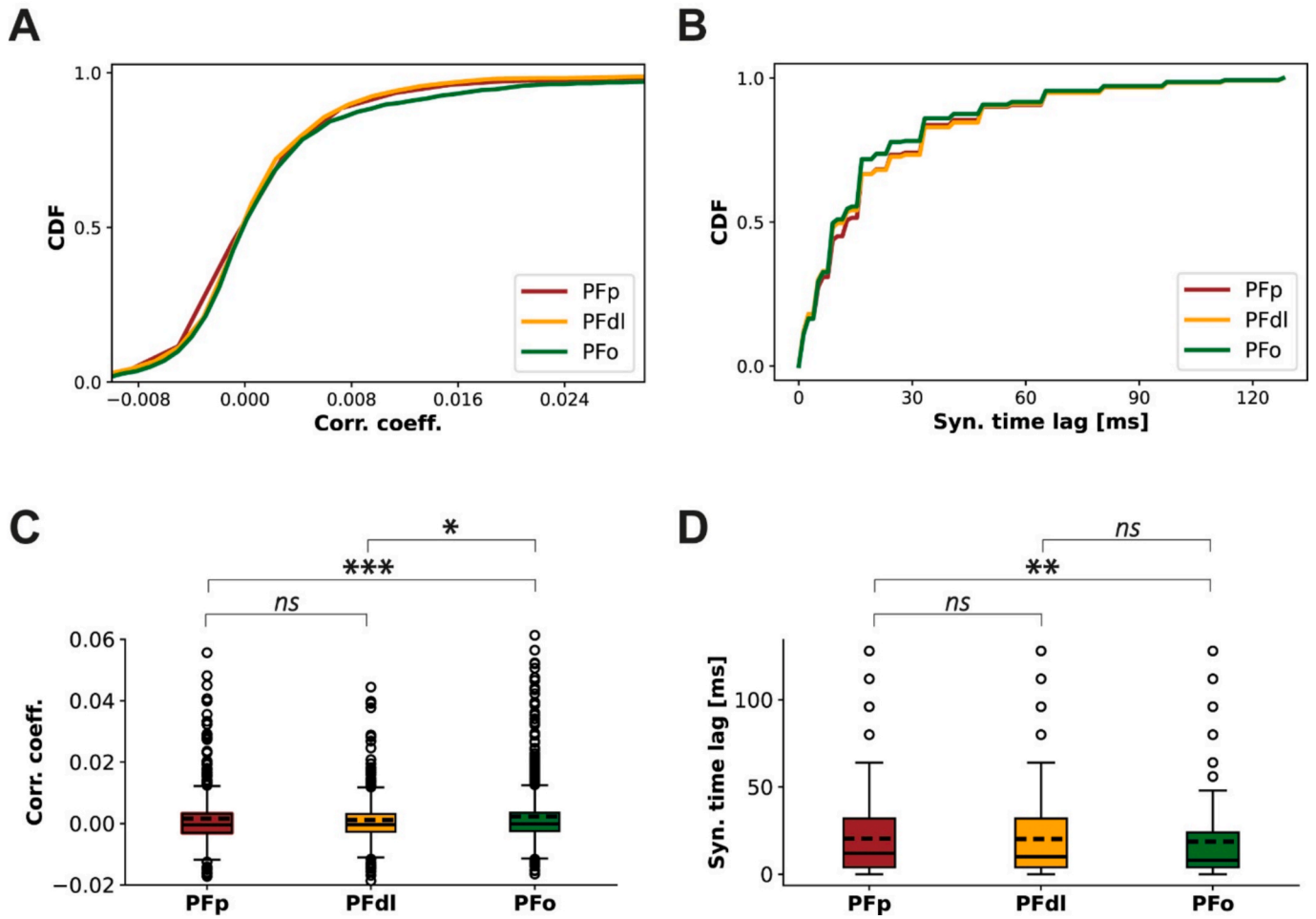

Fig. 4. Robustness. In (**A**) the cumulative density function (CDF) of correlations between pairs of neurons belonging to the same area is measured for all word lengths and letter sizes. In (**B**) the CDF of synchrony time lag between pairs of neurons is shown. Box plots in (**C**) show the distribution of correlations between pairs of neurons. Significant difference (Mann-Whitney U test, $p < 0.05$) between distributions is obtained when comparing PFp and PFdl with PFo. In (**D**), we show the distribution of the synchrony time lag between pairs of neurons belonging to the same area. Significant difference (Mann-Whitney U test, $p < 0.001$) between distributions is obtained when comparing PFp with PFdl and PFo. (**C**) and (**D**) are obtained by aggregating measurements for all combinations of $\Delta\tau$ and W. * $p < 0.05$; ** $p < 0.01$; *** $p < 0.001$; *ns* non-significant.

neuron results, suggesting that the enhanced efficiency in the neural code of both the PFp and the PFdl areas goes beyond the single neuron, and it is a network property.

Trade-off in pairs of neurons

Fig. 6 directly compares the neural code efficiency and robustness of the three prefrontal areas, employing the Pearson correlation coefficient. In particular, we utilized the combined contrast entropy as a measure of efficiency and pair correlation as a measure of robustness. Afterwards, the Pearson correlation coefficient was tested against the null hypothesis of uncorrelated data. If this value was below 0.05, a regression line was plotted. Note that a significant trade-off was observed only when considering the PFo ($p = 1.0\text{x}10^{-7}$). For the purposes of this analysis, outliers that fall outside the 95 % percentile of the χ^2-distribution, as determined by Mahalanobis distance (Mahalanobis, 1936; Baker, 2021), have been excluded.

Discussion

In this work, we examined the three PF areas of the macaque monkey from the perspective of two basic features of the neural code: efficiency, defined as the exploitation of information capacity, and robustness, quantified by correlations and time lags in the neural population. Specifically, we observed higher coding efficiency in PFp and PFdl than in PFo, while PFo showed higher robustness as compared to PFp and PFdl.

To study the coding efficiency, we used the contrast entropy, which is a recent measure designed to quantify the number and statistical occurrence of unique firing patterns observable in neuronal spike trains (Pryluk et al., 2019; Hahn et al., 2024), of which only a subset has been shown to be detectable by other classical measures based on spike train variability (Fano factor and coefficient of variation) (Pryluk et al., 2019). Furthermore, contrast entropy offers an improved control over confounding factors related to intrinsic differences and variations triggered by external events on cell firing rate (Pryluk et al., 2019). Together, these features provide an accurate estimation of the amount of information that can be extracted at the cellular level, underlying the concept of efficiency. We assessed contrast entropy for both individual neurons and neuronal pairs, and in line with previous studies (Pryluk et al., 2019; Hahn et al., 2024), we observed consistently high efficiency levels in all the investigated areas. Such pattern may reflect an energy-efficient coding strategy, where spiking activity is optimized to reduce the metabolic cost during the transmission and processing of information (Baddeley et al., 1997). Coding robustness, conceptualized in this context as the emergence of coordinated and synchronous neuronal activity that may enhance the speed and reliability of downstream information readout (Cohen and Kohn, 2011; Panzeri et al., 2022; Londei

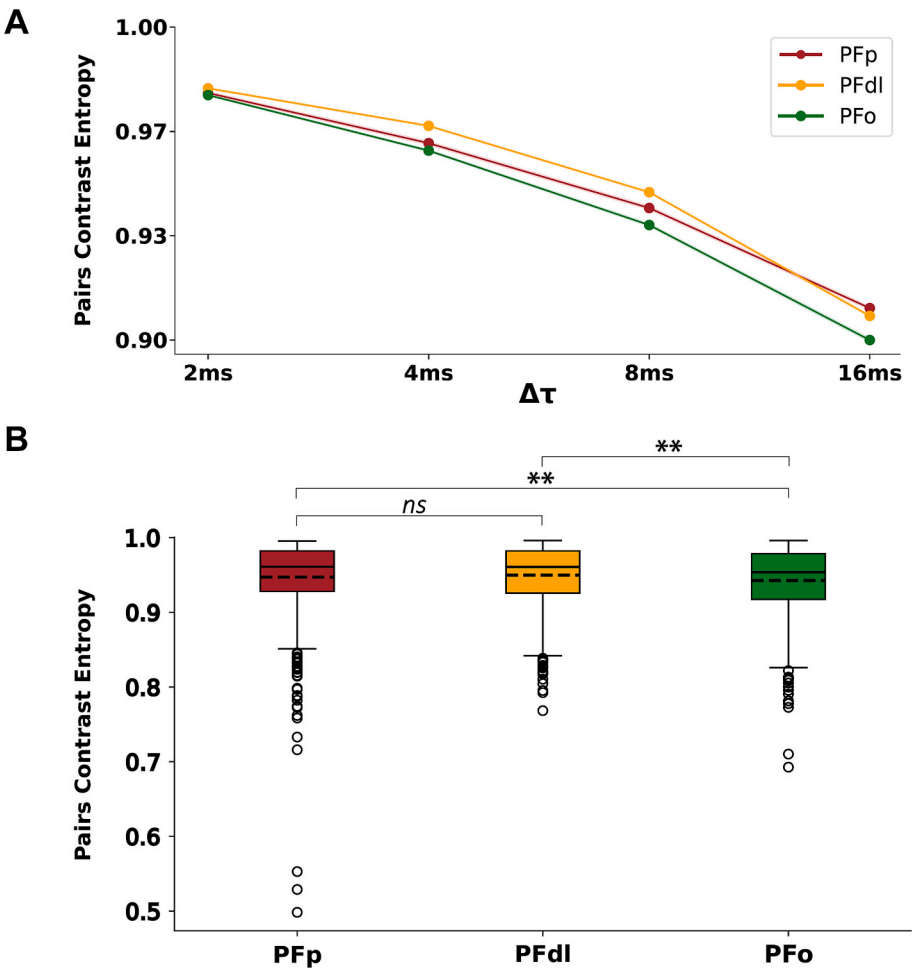

Fig. 5. Pairs contrast entropy, estimated at infinite word length (Strong et al., 1998) with $W = 2, 4, 6, 8$, is illustrated in **(A)**. Higher efficiency is measured for the PFp and the PFdl when compared to the PFo in accordance with the single neuron results. **(B)** Distributions of pairs contrast entropy for each area after aggregating measurements for all values of $\Delta\tau$. Significant statistical difference, according to the Mann–Whitney U test ($p < 0.05$), are observed between PFo and both PFdl and PFp.* $p < 0.05$; ** $p < 0.01$; *** $p < 0.001$; *ns* non-significant.

et al., 2025). We quantified coordination through spike train correlations of simultaneously recorded neurons, and synchrony through time lag in cross-correlation from neuron pairs, consistent with methodologies previously applied by Pryluk et al. (2019).

To date, only two studies have investigated the coding properties in terms of coding efficiency and robustness according to the analytical approaches employed in this study. Pryluk et al. (2019) recorded single neuron spiking activity in the cingulate cortex and amygdala of both humans and macaques, and reported a higher efficiency in human than in monkey neurons at the level of cross-species comparison. In contrast, monkey neurons displayed greater robustness, and at the level of cross-area comparison, a higher efficiency in the cingulate cortex and robustness in the amygdala. Hahn *et al.* (Hahn et al., 2024), using a distinct experimental approach, recorded local field potentials across broad regions of the dorsolateral, medial, and orbitofrontal prefrontal cortex, and hippocampus, in humans and the areas homologous to medial, orbitofrontal prefrontal cortex and hippocampus in rodents during sleep, wakefulness and execution of a visual search task. Their findings confirmed a cross-species difference, with coding efficiency being higher in humans than in rodents, and increased progressively from sleep to task execution. No significant differences were observed among the prefrontal cortices in humans, although efficiency was higher in the prefrontal areas than in the hippocampus. In contrast, rodents showed higher coding efficiency in the medial prefrontal cortex than in the orbitofrontal cortex and hippocampus. Building on this evidence, our study is the first to report differences in both coding efficacy and robustness across prefrontal areas in primates, including PFp, a region unique to anthropoid primates and at the top of the prefrontal hierarchy (Tsujimoto et al., 2010). Given the extreme technical challenges associated with in vivo recordings from PFp (Mitz et al., 2009), studies in primates remain limited (Tsujimoto et al., 2010; Ferrucci et al., 2022a; Nougaret et al., 2024; Ferrucci et al., 2025) and are critical for assessing its role in cognitive processing. The previous studies also helped to contextualize the effect sizes observed in our analyses, regarding statistically significant differences between the areas studied which are consistent with those reported in earlier work using the same metrics for efficiency (Pryluk et al., 2019; Hahn et al., 2024) and robustness (Pryluk et al., 2019), especially when considering that our study relative to the previous ones focuses on the analysis of regions that are part of the same prefrontal cortex. The discrepancy between the significant differences we observed across prefrontal areas and the absence of such differences in Hahn et al. (2024), may reflect a context-dependent effect, as efficiency was measured during task performance in our study and during sleep in the earlier one, contexts that have been shown to influence the magnitude of efficacy values globally (Hahn et al., 2024).

The higher efficiency of PFp and PFdl, coupled with greater robustness of PFo, aligns with the trade-off model proposed by Pryluk et al. (2019), between efficiency and robustness in neural coding, driven by evolutionary pressures. From an evolutionary point of view, the difference between PFp and PFdl from PFo is that the former two probably

evolved later than the latter, i.e., during anthropoid evolution (Passingham and Wise, 2012; Preuss and Wise, 2022). Some of the possible evolutionary pressures during this phase of evolution, as compared to earlier primates, are sporadic food shortages and intense competition, as they foraged over a larger home range and became dependent on the food products of specific trees (Martin, 1981). In life under such pressure, it is critical to avoid unproductive and costly foraging choices and learn to do so quickly based on limited experience. While other groups of sizeable animals solved the problem in their own ways, anthropoids are thought to have solved it in ways that depend on the new granular PF areas, including PFp and PFdl (Passingham and Wise, 2012). In fact, by combining comparative cognitive neuroscience and behavioral ecology, Bouret et al. (2024) showed that the volumes of both PFp and PFdl are explained by daily traveled distance, an index of ecological constraints. This evolutionary interpretation is also supported by the previous laboratory studies on the functional aspects of these areas. PFdl is widely thought of as a central hub for supporting a range of high-level cognitive operations that promote goal-directed behavior in mutable environments. Its functions encompass monitoring previous goals (Barraclough et al., 2004; Genovesio et al., 2006; Seo et al., 2007), their maintenance and manipulation within working memory (Ceccarelli et al., 2025b; Funahashi et al., 1989; Fuster and Alexander, 1971; Benozzo et al., 2024; Londei et al., 2025), and their use to guide endogenous attention (Buschman and Miller, 2007; Everling et al., 2002; Rainer et al., 1998; Di Bello et al., 2025), up to supporting inferential reasoning (Ramawat et al., 2022, 2023) and, together with medial areas and PFp, monitoring others' actions (Barraclough et al., 2004; Hosokawa and Watanabe, 2012; Falcone et al., 2016, 2022; Ferrucci et al., 2022b, 2022a; Franch et al., 2024). Such cognitive processes facilitate the implementation of rules and abstract response strategies that can minimize decision-making errors, contrasting with ancestral learning systems, which rely on slower and simpler adjustments of associative schemes between stimuli, responses, and outcomes, typically resulting in higher error rates before the optimal behavior is achieved (Genovesio and Wise, 2007). Consistent with its demonstrated capacity to integrate multiple sources of information, neuronal populations in PFdl have been shown to represent mixed information simultaneously and dynamically over time, both at the single-cell level and within neuronal assemblies. This capacity reflects a remarkable degree of neural flexibility, which is likely essential for executing complex tasks during goal-directed behavior. Likewise, lesions to PFp were shown to impair only fast learning but not general learning (Boschin et al., 2015), and a recent study provided neurophysiological evidence for the involvement of PFp in the generation of choice and reward size representations during fast associative learning (Nougaret et al., 2024; Ferrucci et al., 2025). These neural functions in PFp and PFdl likely required neural circuits capable of efficiently processing large amounts of information. The enhanced coding efficiency in these areas may reflect an adaptation to support such high-level cognitive processes, which are less critical in the more primitive, agranular PF regions.

In contrast, given that the granular parts of PFo, from which our PFo data were collected, evolved earlier in early primate evolution, the higher robustness observed in the PFo may indicate a relatively retained functionality critical for survival in more immediate, threat-laden environments. In contrast to the anthropoid primates with larger home ranges, the early primates just adapted to a life confined to the fine branches of trees, where they could exploit their tender leaves, fruits, flowers, nectar, and insects (Bloch and Boyer, 2002). Robustness may have ensured reliable behavior and rapid responses to environmental cues in such a life, possibly evidenced in the laboratory as stable, value- and object-based decision-making processes (Wallis, 2007; Rudebeck and Izquierdo, 2022). In a previous study, we also compared the temporal stability of the firing rate across these prefrontal areas, which represent the temporal receptive field of neuronal integration, and found that PFo has a shorter timescale than PFp and PFdl, indicating that information is processed in a shorter time window in PFo than in PFp and PFdl (Fascianelli et al., 2020), in analogy to the faster saturation for the PFo observed in this study.

Another cross-area difference was observed with respect to the within-region tradeoff, i.e., we observed a significant tradeoff in neuron pairs of PFo, but not in those of PFdl and PFp (Fig. 6). This finding seems intriguing, especially when compared to the previous finding of Pryluk et al. (2019), who observed a within-region tradeoff in monkeys, but not in humans. Their recording sites were in the amygdala and cingulate cortex areas, which evolved earlier than the PF regions we focused on here. As in the human brain, the newly incorporated granular PF regions in the macaque monkey may have acquired the advantage of maintaining independence of efficiency and robustness in small local networks, while the granular PFo remained similar to the amygdala and cingulate cortex.

A possible other interpretation of the efficiency/robustness differences, not mutually exclusive with the evolutionary interpretation, might involve the potentially different microcircuitry arrangements in terms of cell typology and properties, axon-dendrite organization, and laminar composition (Pryluk et al., 2019) in the investigated areas, which have shown some intrinsic cytoarchitectural peculiarities (Dombrowski, 2001; Hogeveen et al., 2022). In this context, in a previous study from the same dataset used here, we did not find differences for populations of putative pyramidal neurons and interneurons in the proportions of neurons in these two cell types and in their firing properties across PFp, PFdl, and PFo (Ceccarelli et al., 2025a), which suggests that at least these microcircuit properties may not affect the efficiency/robustness differences reported, in line with what was observed in Pryluk et al. (2019). However, further studies that can model and isolate specific topological network constituents are necessary to assess whether efficiency/robustness may correlate with other differences in the prefrontal microcircuits.

In conclusion, our study highlights the intricate balance between efficiency and robustness in neural coding across different prefrontal cortex areas, reflecting distinct evolutionary adaptations. The higher efficiency in the PFp and PFdl supports advanced cognitive functions necessary for complex, dynamic environments, while the higher robustness in the PFo underscores its role in stable, survival-related behaviors. These findings not only enhance our understanding of the evolutionary development of the primate brain but also provide a framework for exploring the neural basis of cognitive functions and psychiatric disorders. Notably, future studies should investigate whether the trade-off between efficiency and robustness observed in these prefrontal regions and in previously studied areas reflects distinct profiles of functional connectivity with additional interconnected areas, both in terms of connectivity motifs and information coding (Domanski et al., 2023; Harvey et al., 2023; Londei et al., 2024, 2025; Oettl et al., 2020) in normal and pathological conditions.

Data Availability

Spiking data generated from the analyzed dataset are available upon reasonable request from the corresponding author.

CRediT authorship contribution statement

Davide Cipollini: Writing – review & editing, Writing – original draft, Formal analysis, Data curation, Conceptualization. **Fabrizio Londei:** Writing – review & editing, Writing – original draft, Formal analysis, Data curation, Conceptualization. **Satoshi Tsujimoto:** Writing – review & editing, Writing – original draft, Investigation. **Francesco Ceccarelli:** Writing – review & editing, Writing – original draft, Supervision, Data curation, Conceptualization. **Aldo Genovesio:** Writing – review & editing, Writing – original draft, Supervision, Investigation, Conceptualization.

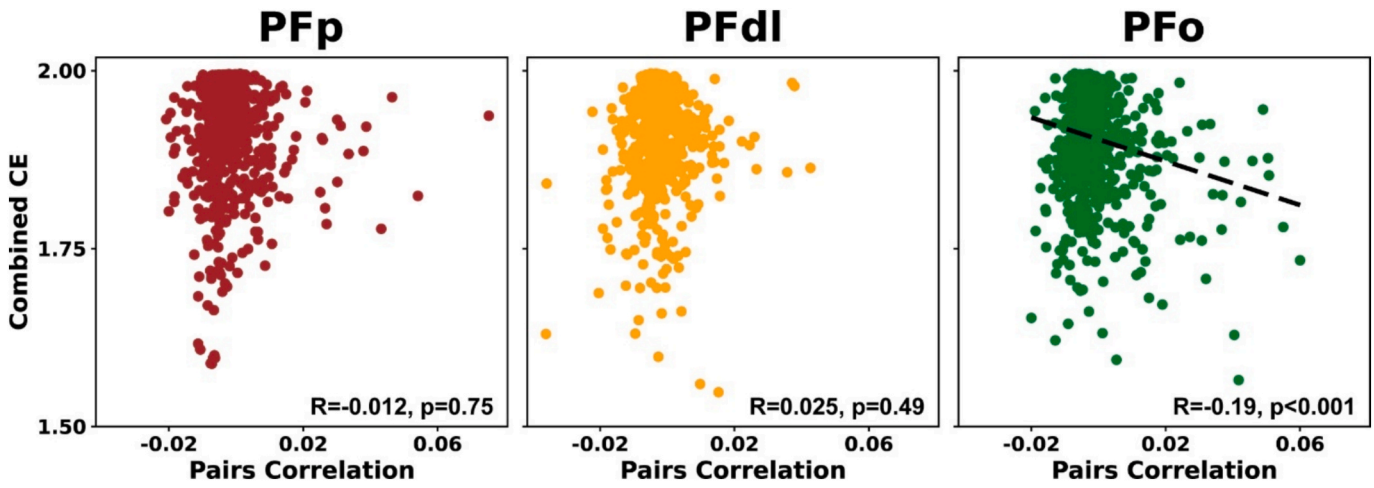

Fig. 6. Trade-off between efficiency and robustness in the three PF areas. The combined contrast entropy is plotted over the pairs correlation. A trade-off between efficiency and robustness ($p < 0.05$) emerges only for PFo (green). Mahalanobis distance is used to compute the p_{χ^2}-values from the χ^2-distribution. Outliers are removed for $p_{\chi^2} < 0.05$. Combined contrast entropy is estimated at infinite word length (Strong et al., 1998), using W = 2, 4, 6, 8 for the linear regression, see Sections 2.5.1, 2.5.2. (For interpretation of the references to colour in this figure legend, the reader is referred to the web version of this article.)

Funding

This study was supported in part by Sapienza University of Rome (Progetto Ateneo 2023: RM123188F6C0E21E to A. Genovesio).

Declaration of competing interest

The authors declare that they have no known competing financial interests or personal relationships that could have appeared to influence the work reported in this paper.

Acknowledgment

We thank Steven P. Wise and Andrew R. Mitz for support during all phases of this project and James Fellows and Ping-Yu Chen for technical support.

References

Baddeley, R., Abbott, L.F., Booth, M.C.A., Sengpiel, F., Freeman, T., Wakeman, E.A., Rolls, E.T., 1997. Responses of neurons in primary and inferior temporal visual cortices to natural scenes. Proc. R. Soc. Lond. B 264, 1775–1783.

Baker, D.H., 2021. Statistical analysis of periodic data in neuroscience. NBDT 5, 1–18.

Barraclough, D.J., Conroy, M.L., Lee, D., 2004. Prefrontal cortex and decision making in a mixed-strategy game. Nat. Neurosci. 7, 404–410.

Benozzo D, Ferrucci L, Ceccarelli F, Genovesio A (2024) History bias and its perturbation of the stimulus representation in the macaque prefrontal cortex. Available at: http://biorxiv.org/lookup/doi/10.1101/2024.10.01.616011.

Bloch, J.I., Boyer, D.M., 2002. Grasping primate origins. Science 298, 1606–1610.

Borst, A., Theunissen, F.E., 1999. Information theory and neural coding. Nat. Neurosci. 2, 947–957.

Boschin EA, Piekema C, Buckley MJ (2015) Essential functions of primate frontopolar cortex in cognition. Proc Natl Acad Sci USA 112 Available at: https://pnas.org/doi/full/10.1073/pnas.1419649112.

Bouret, S., Paradis, E., Prat, S., Castro, L., Perez, P., Gilissen, E., Garcia, C., 2024. Linking the evolution of two prefrontal brain regions to social and foraging challenges in primates. eLife 12.

Buschman, T.J., Miller, E.K., 2007. Top-down versus bottom-up control of attention in the prefrontal and posterior parietal cortices. Science 315, 1860–1862.

Ceccarelli, F., Ferrucci, L., Londei, F., Arena, G., Siano, F., Di Bello, F., Ramawat, S., Tsujimoto, S., Brunamonti, E., Genovesio, A., 2025a. Cell types implement multiple coding schemes in distinct prefrontal cortex areas during goal-directed behavior. Prog. Neurobiol. 251, 102803.

Ceccarelli, F., Ferrucci, L., Londei, F., Ramawat, S., Brunamonti, E., Genovesio, A., 2023. Static and dynamic coding in distinct cell types during associative learning in the prefrontal cortex. Nat. Commun. 14, 8325.

Ceccarelli, F., Londei, F., Arena, G., Genovesio, A., Ferrucci, L., 2025b. Home-cage training for non-human primates: an opportunity to reduce stress and study natural behavior in neurophysiology experiments. Animals 15, 1340.

Cohen, M.R., Kohn, A., 2011. Measuring and interpreting neuronal correlations. Nat. Neurosci. 14, 811–819.

Di Bello, F., Ceccarelli, F., Messinger, A., Genovesio, A., 2025. Endogenous and exogenous attentional interplay through mixed prefrontal cortex resources. Curr. Biol. 35, 3825–3838.e3.

Domanski, A.P.F., Kucewicz, M.T., Russo, E., Tricklebank, M.D., Robinson, E.S.J., Durstewitz, D., Jones, M.W., 2023. Distinct hippocampal-prefrontal neural assemblies coordinate memory encoding, maintenance, and recall. Curr. Biol. 33, 1220–1236.e4.

Dombrowski, S.M., 2001. Quantitative architecture distinguishes prefrontal cortical systems in the rhesus monkey. Cereb. Cortex 11, 975–988.

Everling, S., Tinsley, C.J., Gaffan, D., Duncan, J., 2002. Filtering of neural signals by focused attention in the monkey prefrontal cortex. Nat. Neurosci. 5, 671–676.

Falcone, R., Brunamonti, E., Ferraina, S., Genovesio, A., 2016. Neural encoding of self and another agent's goal in the primate prefrontal cortex: human–monkey interactions. Cereb. Cortex 26, 4613–4622.

Falcone, R., Cirillo, R., Ceccarelli, F., Genovesio, A., 2022. Neural representation of others during action observation in posterior medial prefrontal cortex. Cereb. Cortex 32, 4512–4523.

Fascianelli, V., Battista, A., Stefanini, F., Tsujimoto, S., Genovesio, A., Fusi, S., 2024. Neural representational geometries reflect behavioral differences in monkeys and recurrent neural networks. Nat. Commun. 15, 6479.

Fascianelli, V., Ferrucci, L., Tsujimoto, S., Genovesio, A., 2020. Neural correlates of strategy switching in the macaque orbital prefrontal cortex. J. Neurosci. 40, 3025–3034.

Fascianelli, V., Tsujimoto, S., Marcos, E., Genovesio, A., 2019. Autocorrelation structure in the macaque dorsolateral, but not orbital or polar, prefrontal cortex predicts response-coding strength in a visually cued strategy task. Cereb. Cortex 29, 230–241.

Ferrucci, L., Ceccarelli, F., Londei, F., Arena, G., Elyasizad, L., Nougaret, S., Genovesio, A., 2025. Reward monitoring in the frontopolar cortex of macaques. Sci. Rep. 15.

Ferrucci, L., Nougaret, S., Ceccarelli, F., Sacchetti, S., Fascianelli, V., Benozzo, D., Genovesio, A., 2022a. Social monitoring of actions in the macaque frontopolar cortex. Prog. Neurobiol. 218, 102339.

Ferrucci, L., Nougaret, S., Falcone, R., Cirillo, R., Ceccarelli, F., Genovesio, A., 2022b. Dedicated representation of others in the macaque frontal cortex: from action monitoring and prediction to outcome evaluation. Cereb. Cortex 32, 891–907.

Franch, M., Yellapantula, S., Parajuli, A., Kharas, N., Wright, A., Aazhang, B., Dragoi, V., 2024. Visuo-frontal interactions during social learning in freely moving macaques. Nature 627, 174–181.

Funahashi, S., Bruce, C.J., Goldman-Rakic, P.S., 1989. Mnemonic coding of visual space in the monkey's dorsolateral prefrontal cortex. J. Neurophysiol. 61, 331–349.

Fuster, J.M., Alexander, G.E., 1971. Neuron activity related to short-term memory. Science, New Series 173, 652–654.

Genovesio, A., Brasted, P.J., Wise, S.P., 2006. Representation of future and previous spatial goals by separate neural populations in prefrontal cortex. J. Neurosci. 26, 7305–7316.

Genovesio, A., Wise, S.P., 2007. The Neurophysiology of Abstract Response Strategies. In: Neuroscience of Rule-Guided Behavior (Bunge SA, Wallis JD, eds), pp 0. Oxford University Press. Available at: https://doi.org/10.1093/acprof:oso/9780195314274.003.0006.

Hahn, M.A., Lendner, J.D., Anwander, M., Slama, K.S.J., Knight, R.T., Lin, J.J., Helfrich, R.F., 2024. A tradeoff between efficiency and robustness in the hippocampal-neocortical memory network during human and rodent sleep. Prog. Neurobiol. 242, 102672.

Harvey, R.E., Robinson, H.L., Liu, C., Oliva, A., Fernandez-Ruiz, A., 2023. Hippocampo-cortical circuits for selective memory encoding, routing, and replay. Neuron 111, 2076–2090.e9.
Hogeveen, J., Medalla, M., Ainsworth, M., Galeazzi, J.M., Hanlon, C.A., Mansouri, F.A., Costa, V.D., 2022. What does the frontopolar cortex contribute to goal-directed cognition and action? J. Neurosci. 42, 8508–8513.
Hosokawa, T., Watanabe, M., 2012. Prefrontal neurons represent winning and losing during competitive video shooting games between monkeys. J. Neurosci. 32, 7662–7671.
Londei, F., Arena, G., Ferrucci, L., Russo, E., Ceccarelli, F., Genovesio, A., 2024. Connecting the dots in the zona incerta: a study of neural assemblies and motifs of inter-area coordination in mice. iScience 27, 108761.
Londei, F., Ceccarelli, F., Arena, G., Ferrucci, L., Russo, E., Brunamonti, E., Genovesio, A., 2025. Out of the single-neuron straitjacket: Neurons within assemblies change selectivity and their reconfiguration underlies dynamic coding. J. Physiol. 603, 4063–4090. https://doi.org/10.1113/JP288015.
Mahalanobis P (1936) On the generalized distance in statistics. Available at: https://www.semanticscholar.org/paper/On-the-generalized-distance-in-statistics-Mahalanobis/fa97c2238a16e9226f386ecffe22095e3d3d9dff.
Mansouri, F.A., Koechlin, E., Rosa, M.G.P., Buckley, M.J., 2017. Managing competing goals — a key role for the frontopolar cortex. Nat. Rev. Neurosci. 18, 645–657.
Marcos, E., Londei, F., Genovesio, A., 2019. Hidden markov models predict the future choice better than a PSTH-based method. Neural Comput. 31, 1874–1890.
Martin, R.D., 1981. Relative brain size and basal metabolic rate in terrestrial vertebrates. Nature 293, 57–60.
Miller, E.K., Cohen, J.D., 2001. An integrative theory of prefrontal cortex function. Annu. Rev. Neurosci. 24, 167–202.
Mitz, A.R., Tsujimoto, S., MacLarty, A.J., Wise, S.P., 2009. A method for recording single-cell activity in the frontal-pole cortex of macaque monkeys. J. Neurosci. Methods 177, 60–66.
Nougaret, S., Ferrucci, L., Ceccarelli, F., Sacchetti, S., Benozzo, D., Fascianelli, V., Saunders, R.C., Renaud, L., Genovesio, A., 2024. Neurons in the monkey frontopolar cortex encode learning stage and goal during a fast learning task. PLoS Biol. 22, e3002500.
Oettl, L.-L., Scheller, M., Filosa, C., Wieland, S., Haag, F., Loeb, C., Durstewitz, D., Shusterman, R., Russo, E., Kelsch, W., 2020. Phasic dopamine reinforces distinct striatal stimulus encoding in the olfactory tubercle driving dopaminergic reward prediction. Nat. Commun. 11, 3460.
Panzeri, S., Moroni, M., Safaai, H., Harvey, C.D., 2022. The structures and functions of correlations in neural population codes. Nat. Rev. Neurosci. 23, 551–567.
Passingham, R.E., Wise, S.P. (Eds.), 2012. The Neurobiology of the Prefrontal Cortex: Anatomy, Evolution, and the Origin of Insight. Oxford University Press.
Preuss, T.M., 2001. The discovery of cerebral diversity: an unwelcome scientific revolution. In: Falk, D., Gibson, K.R. (Eds.), Evolutionary Anatomy of the Primate Cerebral Cortex. Cambridge University Press, Cambridge, pp. 138–164.
Preuss, T.M., 2007. Evolutionary specializations of primate brain systems. In: Ravosa, M. J., Dagosto, M. (Eds.), PRIMATE ORIGINS: Adaptations and Evolution. Springer, US, Boston, MA, pp. 625–675.
Preuss, T.M., Goldman-Rakic, P.S., 1991. Myelo- and cytoarchitecture of the granular frontal cortex and surrounding regions in the strepsirhine primate Galago and the anthropoid primate Macaca. J Comp Neurol 310, 429–474.
Preuss, T.M., Wise, S.P., 2022. Evolution of prefrontal cortex. Neuropsychopharmacol 47, 3–19.
Pryluk, R., Kfir, Y., Gelbard-Sagiv, H., Fried, I., Paz, R., 2019. A tradeoff in the neural code across regions and species. Cell 176, 597–609.e18.
Rainer, G., Asaad, W.F., Miller, E.K., 1998. Selective representation of relevant information by neurons in the primate prefrontal cortex. Nature 393, 577–579.
Ramawat, S., Marc, I.B., Ceccarelli, F., Ferrucci, L., Bardella, G., Ferraina, S., Pani, P., Brunamonti, E., 2023. The transitive inference task to study the neuronal correlates of memory-driven decision making: a monkey neurophysiology perspective. Neurosci. Biobehav. Rev. 152, 105258.
Ramawat, S., Mione, V., Di Bello, F., Bardella, G., Genovesio, A., Pani, P., Ferraina, S., Brunamonti, E., 2022. Different contribution of the monkey prefrontal and premotor dorsal cortex in decision making during a transitive inference task. Neuroscience 485, 147–162.
Rieke, F., Warland, D., de Ruyter van Steveninck, R., Bialek, W., 1999. Spikes: exploring the neural code. MIT Press, Cambridge, MA, USA.
Rudebeck, P.H., Izquierdo, A., 2022. Foraging with the frontal cortex: a cross-species evaluation of reward-guided behavior. Neuropsychopharmacol 47, 134–146.
Selemon, L.D., Zecevic, N., 2015. Schizophrenia: a tale of two critical periods for prefrontal cortical development. Transl. Psychiatry 5, e623–e.
Seo, H., Barraclough, D.J., Lee, D., 2007. Dynamic signals related to choices and outcomes in the dorsolateral prefrontal cortex. Cereb. Cortex 17, i110–i117.
Shannon, C.E., 1997. The mathematical theory of communication. 1963. M.D. Comput. 14, 306–317.
Smucny, J., Dienel, S.J., Lewis, D.A., Carter, C.S., 2022. Mechanisms underlying dorsolateral prefrontal cortex contributions to cognitive dysfunction in schizophrenia. Neuropsychopharmacol 47, 292–308.
Strong, S.P., Koberle, R., de Ruyter van Steveninck, R.R., Bialek, W., 1998. Entropy and information in neural spike trains. Phys. Rev. Lett. 80, 197–200.
Treves, A., Panzeri, S., 1995. The upward bias in measures of information derived from limited data samples. Neural Comput. 7, 399–407.
Tsujimoto, S., Genovesio, A., 2017. Firing variability of frontal pole neurons during a cued strategy task. J. Cogn. Neurosci. 29, 25–36.
Tsujimoto, S., Genovesio, A., Wise, S.P., 2009. Monkey orbitofrontal cortex encodes response choices near feedback time. J. Neurosci. 29, 2569–2574.
Tsujimoto, S., Genovesio, A., Wise, S.P., 2010. Evaluating self-generated decisions in frontal pole cortex of monkeys. Nat. Neurosci. 13, 120–126.
Tsujimoto, S., Genovesio, A., Wise, S.P., 2011. Comparison of strategy signals in the dorsolateral and orbital prefrontal cortex. J. Neurosci. 31, 4583–4592.
Tsujimoto, S., Genovesio, A., Wise, S.P., 2012. Neuronal activity during a cued strategy task: comparison of dorsolateral, orbital, and polar prefrontal cortex. J. Neurosci. 32, 11017–11031.
Walker, A.E., 1940. A cytoarchitectural study of the prefrontal area of the macaque monkey. J of Comparative Neurology 73, 59–86.
Wallis, J.D., 2007. Orbitofrontal cortex and its contribution to decision-making. Annu. Rev. Neurosci. 30, 31–56.
Wise, S.P., 2008. Forward frontal fields: phylogeny and fundamental function. Trends Neurosci. 31, 599–608.
Wong, P., Kaas, J.H., 2010. Architectonic subdivisions of neocortex in the galago (Otolemur garnetti). Anat. Rec. 293, 1033–1069.